СООБЩЕНИЯ
ОБЪЕДИНЕННОГО
ИНСТИТУТА
ЯДЕРНЫХ
ИССЛЕДОВАНИЙ
ДУБНА

E14 - 9206

K.Feldmann, K.Hennig, W.Matz, M.Müller,
J.Schreiber, L.Weiss

NEUTRON SCATTERING INVESTIGATIONS ON FeMnNi (Be) ALLOYS

1975

E14 - 9206

K.Feldmann[1], K.Hennig, W.Matz, M.Müller[2],
J.Schreiber, L.Weiss[1]

NEUTRON SCATTERING INVESTIGATIONS ON FeMnNi (Be) ALLOYS

[1] Zentralinstitut für Kernforschung, Rossendorf, GDR.
[2] Zentralinstitut für Festkörperphysik und Werkstofforschung, Dresden, GDR.

1. Introduction

Neutron elastic and inelastic scattering data have been obtained from several samples of FeMnNi(Be) antiferromagnetic alloys. The samples differ in their degree of cold working, annealing procedure and beryllium content. Besides the disordered γ-f.c.c.-antiferromagnetic phase the precipitated NiBe phase (CsCl structure) exists in samples which are annealed at higher temperatures. Neutron diffraction results obtained on binary FeMn and ternary FeMnNi-alloys are reported in /1-5/. Our diffraction patterns contain peaks due to the NiBe phase and inelastic neutron scattering spectra show in addition to the broad phonon spectrum localized modes of Be and peaks due to magnons of rather high energy.

2. Experiments

The experiments were performed at the pulsed reactor IBR-30 of the JINR using the time-of-flight method. The elastic and inelastic spectra were obtained at 300 K with a soller collimator or nitrogen cooled beryllium filter in front of the detector (inverted geometry), respectively /6,7/. In both cases the first flight path (moderator-sample) and the second flight path (sample-detector) were 30.6 m and 1.1 m, respectively. Six polycrystalline samples, size 160 x 100 x 5 mm^3, were prepared in the Zentralinstitut für Festkörperphysik und Werk-

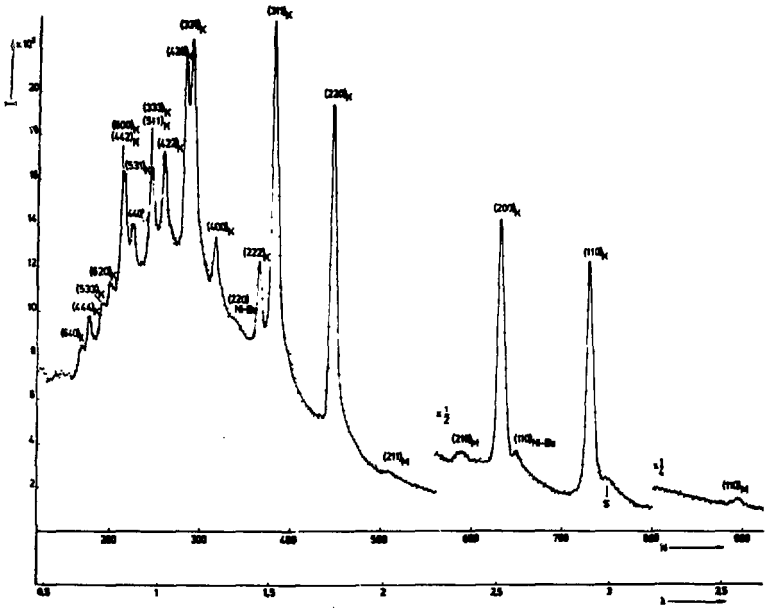

Fig. 1. Spectrum of elastically scattered neutrons FeMnNi(Be) *-alloy (sample 5) .* I *- counts per 5 hours and channel.* N *- channel number (width 32* μ*sec).* λ *-wavelength of neutrons in* Å .

stofforschung. Sample 1 and 2 contain 60 at.% Fe , 30.5 at.% Mn and 9.5 at.% Ni and samples 3,4,5 and 6 56.0 at.% Fe , 29.2 at.% Mn , 9.1 at.% Ni and 4.8 at.% Be. All samples are homogenized at 1060°C for 1 hour and quenched in water. The samples 4, 5 and 6 are annealed at 500, 600 and 700 ° C, respectively, for 1 hour in hydrogen atmosphere and cooled by air. Figure 1 shows the time-of-flight diffraction spectrum at a scattering angle of 90° for the 5 th sample. Nuclear peaks of the γ -phase are signed by K and magnetic peaks by M . Diffraction peaks due to the precipitated phase NiBe are also seen. S - denotes satellites, which are caused by fast neutrons.

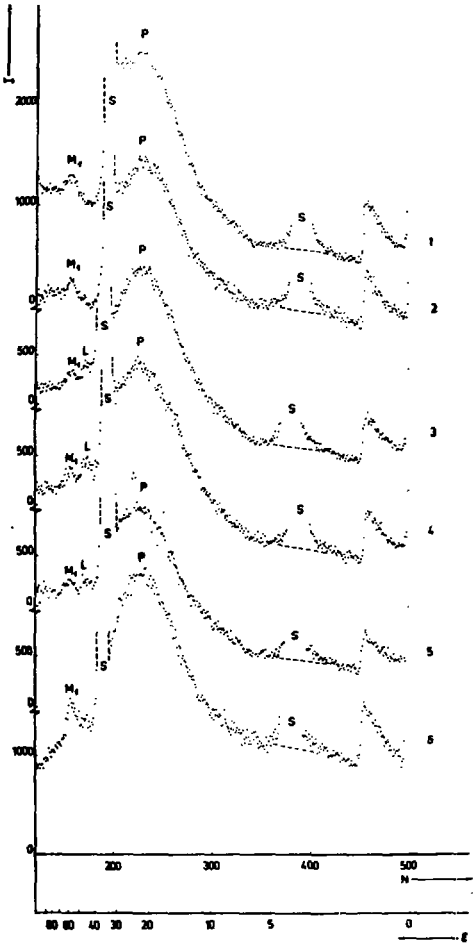

Fig. 2. Time-of-flight spectra of inelastically scattered neutrons on FeMnNi (Be) *-alloys at 90° scattering angle. The numbers at spectra indicate the sample number.* I *- counts per 20 hours and channel.* N *-channel number (width 64* μ*sec).* ε *- energy loss of neutrons in meV.*

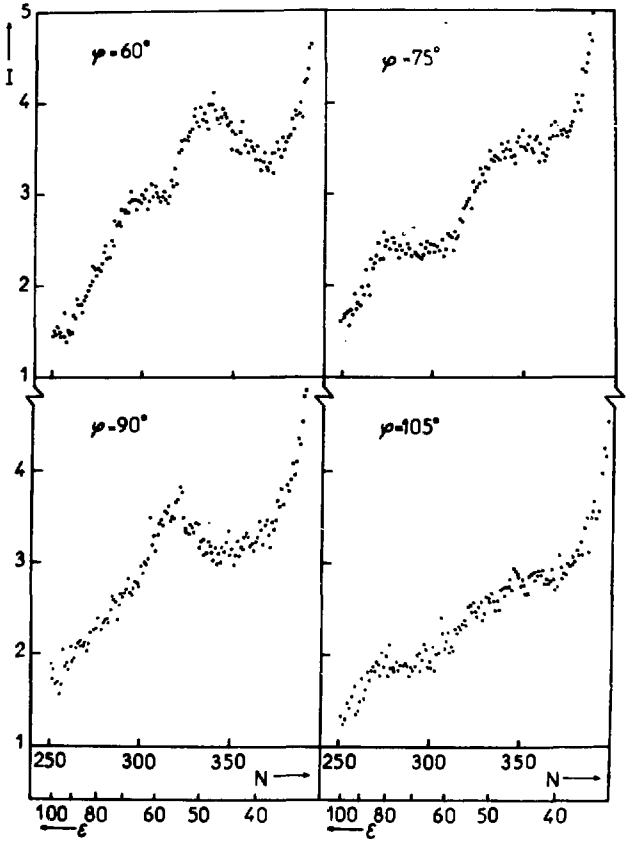

Fig. 3. Time-of-flight spectra of inelastically scattered neutrons from sample 1 at 60, 75,° 90°and 105 ° . The spectra are corrected for background and intensity of incident neutron spectrum. I - intensity per channel in arbitrary units. N - channel number (width 32 μsec). ε - energy loss of neutrons in meV.

Inelastic spectra are measured at different scattering angles. In Fig. 2 the spectra for all samples measured at a scattering angle of 90 ° and room temperature are

shown. The data have been corrected for constant background and normalized. The beryllium cut-off appears at the channels number 495. The small cut-off at N =450 is also caused by the beryllium filter. The very high peaks are due to the so-called satellites. All spectra show a broad peak P at N = 230 (ϵ = 21±2 meV) and at N = 155 (ϵ = 58±3 meV) the peak M_1. The spectra from samples 3,4,5 show an additional peak L at N = 170 (ϵ = 46±3 meV). Figure 3 shows parts of the inelastic spectra from sample 1 obtained at room temperature and scattering angles ϕ = 60°, 75°, 90° and 105° . The data have been also corrected for constant background and the incident neutron spectrum. At the right side the spectra parts are limited by satellites.

3. Discussion

According to the special antiferromagnetic structure of the γ -phase, having 4 spins in the unit cell aligned in the four different [111] directions [1,5], there appear pure magnetic (e.g., (110), (210), (211)) and pure nuclear Bragg reflections (e.g., (111), (200), (220)). In addition, the (110) and (220) reflections of the NiBe phase can be seen, Fig. 1, while the expected (200) peak overlaps with the wing of the strong (220) peak of the γ -phase. Other samples with the similar concentrations have been studied by the conventional neutron diffraction at Zentralinstitut für Kernforschung. The amount of the NiBe phase was qualitatively determined by comparison of the integrated intensities of the (200) NiBe peak with the (220) γ -phase peak. It was found that for cold-worked samples (61.5% deformation) strong precipitation of NiBe occurs for annealing temperature above 600°C. Without coldworking the annealing temperature must be rised by 50 ÷ 100° C in order to obtain the same amount of NiBe . The temperature dependence (77 K - 480 K) of the mean magnetic moment was fitted with a Brillouin function. For $T > T_N$ the magnetic moment did not disappear (~ 5% left), what can be interpreted as being due to the short range order,

or inhomogenity of the composition of the alloy, as it is discussed in [4]. Figure 1 presents no indication of any other phase than the γ-phase and Ni Be phase. This was also confirmed by all other time-of-flight and conventional diffraction pattern of the sample used.

In the spectra of inelastically scattered neutrons, Fig.2, the peak denoted by L and localized above the upper phonon excitation energy limit at ϵ = 36 meV, is missing in the beryllium free samples 1 and 2, while it exists in samples 3,4 and 5 and gets smaller in the 6th sample. Therefore we are interpreting this peak L as a localized vibrational mode of solved Be atoms in the FeMnNi matrix. For other investigations of excitations of light impurity atoms in a matrix of heavier atoms see, for example, Be in Cu [8].

The broad phonon peak is the superposition of phonons of the γ-and Ni Be -phase. The phonon cut-off energy ϵ_{Ph} is in agreement with approximate estimations obtained using Debye temperatures: Θ_γ = 425 K, ϵ_γ = 36.6 meV and $\Theta_{Ni\,Be}$ = 307 K, $\epsilon_{Ni\,Be}$ = 26.5 meV [4]. The inelastic scattering contributions of the γ-phase result mainly from coherent inelastic scattering processes from (111) and (200) reflections [10].

In order to get more information about the peak M_1 in the 90° spectra (Fig. 2) further measurements at scattering angles ϕ = 60°, 75°, 90°, 105° and 120° were made on the beryllium free sample (Fig. 3). With increasing scattering angle the peak intensities become smaller. Additional experiments on a sample temperature T = 500 K > T_N (T_N = 380 K) at ϕ = 90° and 60° show an increasing of the intensity of the phonon hump while the higher energy peaks vanish. From the dependence of the intensity on temperature and scattering angle the peaks in the energy range from 40 to 80 meV can be attributed to magnon scattering. This can be understood as a coherent inelastic process with a momentum transfer $\vec{q}$ to the magnons.

$$2\pi\vec{\tau}_{hk\ell} - \vec{q}_{max} \leq \vec{Q} = 2\pi\vec{\tau}_{hk\ell} + \vec{q} \leq 2\pi\vec{\tau}_{hk\ell} + \vec{q}_{max} \qquad (1)$$

with $|\vec{q}_{max}| = \pi/a = 0.87\ \text{Å}^{-1}$ the wave vector of the

magnons at the zone boundary and $\vec{\tau}_{hkl}$ the reciprocal lattice vector. For a more quantitative interpretation of our results we have to look for a suitable model, which can sufficiently explain the found magnon peaks. According to /2/ the properties of $Fe_{60}Mn_{30}Ni_{10}$ can be explained by a model which contains the so-called "induced moments" (caused by the band antiferromagnetism of Fe–Mn) and "permanent moments" (localized spins at Ni -sites). Just this features can be described by the modified Zener model (MZM) /11-14/ which has recently used to explain the properties of ferromagnetic $Fe_{65}(Mn_xNi_{1-x})_{35}$ /12,13/. In /11/ it was shown that antiferromagnetism occurs in the MZM if the concentration of itinerant Zener electrons (or holes) is high enough. Since in our system Fe and Mn give only collective Zener holes /2/ , we could therefore accept the validity of MZM for our antiferromagnetic sample. If the influence of the localized moments increases as a consequence of increasing Ni -concentration, a change of the ground state from antiferromagnetism to ferromagnetism occurs /2/. To the authors knowledge so far spin wave calculations for antiferromagnetic MZM were not made although an extension of the RPA theory for the ferromagnetic system /13/ to the antiferromagnetic one is possible without general difficulties. One of the interesting features of the MZM is the appearance of acoustical and optical magnons, because of the existence of two subsystems: the itinerant electron and the localized moment system. Regarding this circumstance we can expect that also in the here considered system both spin wave branches are present. According to the antiferromagnetic ordering in each subsystem, the following dispersion relations for small q -values will be expected:

$$\omega_{op} = c_{op}q + \omega_q$$
$$\omega_{an} = c_{ac}q + \omega_{an} \qquad (2)$$

(ω_q - optical gap; ω_{an} - gap produced by anisotropy fields). In ferromagnetic system the optical branch was not observed until now, since ω_q is too high for neutron experiments or is lying in the Stoner continuum /13,14/ .

However, in the considered antiferromagnetic system the effect of the localized moments is much smaller because of the small amount of Ni -atoms. Hence the optical gap should be small enough, so that optical magnons could be observed in $Fe_{60}Mn_{30}Ni_{10}$ system.

In order to interprete our experimental results in the framework of this model, we must take into account two more facts. At first we can only work with (2) in the first part of the Brillouin zone, since otherwise Stoner excitations in our metallic system can destroy magnons. On the other hand we assume isotropic dispersion relations. because bandantiferromagnetism (like FeMn /15/) shows an isotropic dispersion of acoustical spin waves and the slope of the optical branch should be small, so that splitting of the dispersion in different directions should be not important. Thus we can expect well separated magnon peaks also in polycrystalline materials.

Assuming, that the dispersion curves begin at the magnetic Bragg-reflections (210), (211), (300), (310), (320) and (321), we have finally found a satisfactory explanation of our experimental results in sense of (2) with the parameter set.

$$c_{op} = 1.53.10^3 ms^{-1} \qquad \omega_q = 70 \text{ meV}$$

$$c_{ac} = 1.75.10^4 ms^{-1} \qquad \omega_{an} = 5 \text{ meV} .$$

The phase velocity of the acoustic antiferromagnons is of the common order /9/ . Possible acoustic magnon peaks from (110) and (210) reflections with low energies overlap with the broad phonon peak P and therefore cannot be seen.

4. Summary

The diffraction data show that the investigated Be -containing Fe Mn Ni -alloys consist of the disordered f.c.c. γ -phase and the Ni Be -phase, where the concentration of the latter depends on the annealing temperature and the degree of cold-working. Inelastic scattering experiments show that the Be atoms in the γ -phase causes the localized modes with excitation energy $\epsilon_L =$

46 meV, while the phonon cut-off-energy $\epsilon_C \approx 36$ meV. Peaks at energies higher than ϵ_L and ϵ_C are interpreted as excitations due to acoustic and optical antiferromagnons. This can be explained with the help of the modified Zener model in which the two magnon branches are caused by two inequivalent subsystems: the localized moments of Ni and the itinerant electrons of Fe and Mn.

The authors would like to express their thanks to Dr. B.Lippold for experimental assistance and Dr. Yu.M.Ostanevich for stimulating discussions.

References

1. *Y.Nakamura, M.Shiga, Y.Takeda. J.Phys.Soc.Japan, 27, 1470 (1969).*
2. *M.Shiga. J.Phys.Soc.Japan, 22, 539 (1967).*
3. *Y.Ishikawa, Y.Endoh. J.Appl.Phys., 39, 1318 (1968).*
4. *Y.Ishikawa, E.Endoh. J.Phys.Soc.Japan, 23, 205 (1967).*
5. *H.Umebayashi, Y.Ishikawa. J.Phys.Soc.Japan, 21, 1281 (1966).*
6. *V.B.Zlokazov, B.N.Savenko, K.Hennig, JINR, P14-6731, Dubna, 1972.*
7. *K.Parlinski, M.Sudnik-Hrynkiewicz, A.Bajorek, T.A.Janik, W.Olejarczyk. in: Research Applications of Nulcear Pulsed System, IAEA, Vienna 1967, p. 179.*
8. *I.Natkaniec, K.Parlinski, J.A.Janik, A.Bajorek, M.Sudnik-Hrynkiewicz. in: Neutron Inelastic Scattering (Proc. Symp. Copenhagen 1968) vol. I, p. 65, IAEA, Vienna 1968.*
9. *T.Riste, J.A.Goedkoop. Nature, 185, 450 (1960).*
10. *K.E.Larsson, in: Neutron Inelastic Scattering (Proc. Symp. Copenhagen 1968) vol. I, p. IAEA, Vienna 1968.*
    P.A.Egelstaff. AERE-Report R 4101 (1962).
11. *T.Asai. Phys.Rev.Lett., 27, 1226 (1971).*
12. *L.R.Edwards, L.C.Bartel. Phys.Rev., B10, 2044 (1974).*
13. *L.C.Bartel. Phys.Rev., B7, 3153 (1973); Phys.Rev., B8, 5316 (1973).*
14. *I.S.Tyagi, R.Kishore, S.K.Joshi. Phys.Rev., B10, 4050 (1974).*
15. *Y.Endoh, E.Shirane, Y.Ishikawa, K.Tajima. Solid State Commun., 13, 1179 (1973).*

Received by Publishing Department
on September 30, 1975.